Shirshov Institute of Oceanology, Russian Academy of Sciences, 117997, Nahimovskiy prospekt, 36, Moscow, Russia
*E-mail: pereslegsv@yandex.ru

# THE MODEL OF RADAR OBSERVATION OF THE SURFACE VIBRATION WAVES GENERATED BY EARTHQUAKE SOURCE (GROUND VIBRATOR)

Received 27.05.2021, revised 18.10.2021, accepted 20.12.2021

**Abstract**

This research article is continuation case study based on a model of radar monitoring of vibration waves occurring on the sea surface near the source of a bottom earthquake. The vibration wave is generated parametrically, has near (hydrodynamic) and far (sound) components. The amplitude of the near (generating) wave depends on the bottom vibrator parameters and the depth of the bottom, the far wave propagates in the waveguide formed by the surface and the flat bottom. The vibrator will be installed at a shallow depth (30 m) and the modern aircraft radar will be used to create amplitude and velocity radar images during the experiment. The length of the generated vibration wave will be ~1.5 cm, which corresponds to the frequency of the generating wave ~30 Hz and the "resonant" wave of the radar with a length of ~3 cm (radar X-band). The possibility of monitoring vibration waves in the amplitude and velocity channels of the SAR (synthetic aperture radar) in L, P and UHF-bands is estimated. Also, the expected view of the SAR images is shown. Calculations of the necessary parameters of the aircraft radar are provided, including algorithms for processing the initial signal when creating amplitude and velocity radar images of vibration waves.

**Keywords**: bottom vibrator, near and far pressure fields, sound waveguide, vibration wave on the background of wind waves, amplitude and velocity radar images



Институт океанологии им. П.П. Ширшова РАН, 117997, Нахимовский пр., д. 36, г. Москва, Россия
*E-mail: pereslegsv@yandex.ru

# МОДЕЛЬ РАДИОЛОКАЦИОННОГО НАБЛЮДЕНИЯ ВИБРАЦИОННЫХ ПОВЕРХНОСТНЫХ ВОЛН, ВОЗБУЖДАЕМЫХ ИСТОЧНИКОМ ЗЕМЛЕТРЯСЕНИЙ (ДОННЫМ ВИБРАТОРОМ)

Статья поступила 27.05.2021, после доработки 18.10.2021, принята в печать 20.12.2021

**Аннотация**

Продолжая исследования, опубликованные ранее [1], рассматривается модель радиолокационного мониторинга вибрационных волн, возникающих на морской поверхности вблизи очага донного землетрясения. Возбуждаемая параметрически вибрационная волна характеризуется ближней (гидродинамической) и дальней (звуковой) областями. Амплитуда ближней волны зависит от параметров донного вибратора и глубины дна, дальняя распространяется в волноводе, образованном водной поверхностью и плоским дном. Намечаемый натурный эксперимент предполагает установку вибратора на небольшой глубине (30 м) и применение современного самолётного радара, способного формировать как яркостные, так и скоростные радиолокационные изображения слабо отражающей морской поверхности при длине возбуждаемой вибрационной волны ~1,5 см, что соответствует частоте возбуждающей волны ~30 Гц и «резонансной» радиоволне длиной ~3 см (радиолокационный X-диапазон). Рассматривается возможность наблюдения вибрационных волн в радаре с синтезированной апертурой в L, P и УКВ-диапазонах. Приводятся также расчёты, относящиеся к необходимым параметрам самолётного радара с синтезированной апертурой, включая алгоритмы обработки исходного сигнала при формировании яркостных и скоростных радиолокационных изображений вибрационных волн.

**Ключевые слова:** донный вибратор, ближнее и дальнее поля давления, звуковой волновод, вибрационная волна на фоне ветровых волн, яркостное и скоростное радиолокационные изображения

Ссылка для цитирования: *Карпов И.О.*, *Переслегин С.В.* Модель радиолокационного наблюдения вибрационных поверхностных волн, возбуждаемых источником землетрясений (донным вибратором) // Фундаментальная и прикладная гидрофизика. 2022. Т. 15, № 1. С. 48–60. doi: 10.48612/fpg/naz1-x7da-r4gn
For citation: *Karpov I.O.*, *Pereslegin S.V.* The Model of Radar Observation of the Surface Vibration Waves Generated by Earthquake Source (Ground Vibrator). *Fundamental and Applied Hydrophysics*. 2022, 15, 1, 48–60. doi: 10.48612/fpg/naz1-x7da-r4gn

## 1. Introduction

In our work [1] the effect of parametric excitation of the surface wave from harmonic source of vibration, installed on the bottom of shallow water, was considered. It was noted that in the nearest area from the vibrator can be ignored the fluid compressibility. That means that to adopt a hydrodynamic justification of the considered effect. Laboratory experiment, conducted in the depths of the bath $H$ = 15 cm and the frequency of the vibrator $F_s$ = 30 Hz showed that on the surface, in accordance with the theories of parametric excitation [2, 3] — over the vibrator, around a small spot of standing waves ("Faradei ripples") a circle-running wave produces with a frequency $F_v$ = 15 Hz and lenth $\Lambda_v$ ~ 1.5 cm — in accordance to the dispersion relation for gravitational-capillary waves. This wave was displayed as a "resonant" at the output of the phase detector of the laboratory radar, at the amplitude of fluctuations with a wide spectrum $\delta F$ ~ 2 Hz which should be attributed to the "parametric instability" effect.

When changing from a laboratory experiment to an *in-situ* experiment, where the depth of the water and the distance from the vibrator are comparable to the length of the sound wave (and in many cases much exceed it), one has to rely on the idea of an acoustic field, in particular the acoustic pressure field in the waveguide formed by the "hard" bottom and "soft" water surface. Unfortunately, recently published in national works [4, 5], devoted to the problems of sound distribution — this is a question that, in our view, is not satisfactorily considered, therefore we turned to the classic work of M.A. Isakovich [6], where the expressions for the field of pressure in the liquid are given — as in the case of a flat wave in the waveguide (§ 70), so and in the case of cylindrical wave (§ 80), bounded by a hard wall (bottom) and a soft wall (surface).

Artificial vibration source installed on the bottom of "sea polygon" type of MHI RAS polygon (Katsiveli, Crimea) is to be used in the planned *in-situ* experiment. In this case, the depth of the water is $H$ ~ 30 m, and the vibration frequencies must correspond to the lengths of the waves of the aircraft or space radar. Calculations, as well as the resulting high-speed images from the foreign-operated aircraft radar [7] and space radar (Tandem Terra SAR-X [8]) show that a similar source of vibration must be visible in the background of wind waves. There is also a domestic (four-band) aircraft SAR complex, dedicated to "surface and subsurface sensing" [9]. The proposed experiment should help to solve the problem of earthquake site of origin radar monitoring, where the frequency spectrum of the vibration is wide and repeatedly measured with the help of ground seismometers [10]. Finally, it is necessary to determine the parameters of the formed SAR images and the necessary parameters of the SAR equipment, including its power supply.

Thus, this work is multidisciplinary. That contains calculations combining known works on the problems of hydrophysics, hydroacoustics and radiophysics (there are types of work [11,12] on the formation of velocity radar images). The purpose of this work is the justification of the planned *in-situ* experiment on radar observation of surface vibration waves excited by a ground vibrator.

## 2. Ground harmonic vibrator, its pressure field (closer and farther areas)

Before turning to the radar of bottom earthquakes, consider the existing understanding of their source — the bottom vibrator. The pressure in the environment above the vibrator was calculated on the assumption that the size of the vibrating membrane was small compared to the length of sound wave: $d / \Lambda_s << 1$, $\Lambda_s = c / F_s$, $F_s$ — frequency of vibration, $c$ — speed of sound in water. In this case, when using hydrodynamic representations, the directivity pattern of the source is a hemisphere, where the vertical component of the amplitude of the pressure is:

$$p_m = \frac{\rho d^2 b_m \omega^2 \cos\theta}{32\pi H} = \frac{\pi\rho d^2 b_m F_s^2 \cos\theta}{8H}. \quad (1)$$

Here $H$ is the depth of the water, $d$ is the diameter of the bottom membrane, vibrating with the amplitude of $b_m$, $\theta$ = arctg $(x/H)$, $x$ is the horizontal distance from the point over vibrator [1].

The concept of the distribution of sound waves leads to the fact that between the "hard" bottom and "soft" water surface there exists a waveguide, which is activated by a bottom vibrator at the amplitude of pressure (1). In this case, the sound wave can be spread along the waveguide only under the condition that its frequency is higher than the "critical" frequency, determined by $F_s^* = \frac{c}{4H}$. It means that at the length of the sound wave less

than a quarter of the depths of the bottom. At $F_s > F_s^*$ there is a solution for sound pressure along the waveguide, taking both walls flat. Cylindrical coordinates (*z, x*) are used and horizontal and vertical wave numbers are introduced ($\chi$, $\zeta$), different from the wave number in the free environment $k = 2\pi F_s/c$, and $k^2 = \chi^2 + \zeta^2$:

$$p(z,x) = p_m(x)\sin(\varsigma z + \omega t)\, H_0^{(1)}\left(kx\sqrt{1-\frac{\varsigma^2}{k^2}}\right). \quad (2)$$

The value of $p_m(x)$ is determined by the expression (1), and $H_0^{(1)}(k,x)$ is Hankel function of the first kind (order zero), which determines the pressure amplitude decreasing with the growth of the horizontal coordinate *x*. Axis z is directed downwards. Accept that $z = H$, and for a sound wave, which is distributed along the waveguide along the *x* axis, calculate the module of the function (2) at $\sin(\zeta z) = 1$. The signal stays harmonious, but it considered only its spatial components. The value $\varsigma = \frac{\pi}{2H}(2n-1)$, $n = 1,2...$ is the vertical wave number, which is taken the smallest ($n = 1$) [6]. When the intensity detector is placed at the surface at different points on the *x* axis, the calculated expression for the amplitude of the pressure is:

$$p(x) = p_m(x)\left|H_0^{(1)}(x)\right| \times \left|\mathrm{Re}\left(H_0^{(1)}(x)\right)\right|, \quad (3)$$

$$\text{where } H_0^{(1)}(x) = H_0^{(1)}\left(\frac{2\pi F_s x}{c}\sqrt{1-\left[\frac{c}{4HF_s}\right]^2}\right). \quad (4)$$

In this way, it is taken that near $p_m(x)$ and far (sound) components of the wave, which is distributed around the bottom vibrator. At frequencies $F_s < c/4H$ the sound wave is not distributed along the waveguide, and the module of the Hankel function (4) should be calculated only for the far region at $F_s > c/4H$ and $x > 4H/2\pi$.

Further, it is necessary to agree the data obtained with the conditions, typical for modern methods of sea surface radar sensing. In this case, there means a side-looking radar with a real or synthetic aperture (RAR or SAR), the wavelength of which is strongly associated with the length of the vibration wave formed on the surface. Let's consider the angle of the radar visualization of the surface is grazing angle ($\gamma \geq 60°$), then the length $\Lambda_v$ of the vibrating wave must be half the length $\lambda$ (a "resonant" radio wave $\lambda = 2\Lambda_v$). The frequency of the surface vibration is assumed half the frequency of vibration, which follows from the conducted experiment [1]: $F_v = F_s/2$. This frequency corresponds to the length $\Lambda_v$ that's behave to dispersion equation $\omega_v = \left(gk_v + \sigma\frac{k_v^3}{\rho}\right)^{1/2}$, where $k_\nu = \frac{2\pi}{\Lambda_\nu}c^{-1}$, $\sigma = 75\ \mathrm{g}\cdot s^{-2}$ — a surface tension. At frequencies $F_v \leq 10$ Hz should be ignored of surface tension. Then a simple relationship will be gotten, where the observed radar frequency of the vibrating membrane is determined by the length of the radar radio wave:

$$F_s = 2\sqrt{\frac{g}{\pi\lambda}}. \quad (5)$$

Taking into account the domestic aircraft SAR complex [9], from the expressions (5) are obtained the following (necessary) frequencies of vibration:

*a*) X-range, $\lambda = 3.1$ cm, $F_s = 28$ Hz (taking into account of surface tension);
*b*) L-range, $\lambda = 23$ cm, $F_s = 7.4$ Hz;
*c*) P-range, $\lambda = 90$ cm, $F_s = 3.7$ Hz;
*d*) UHV-range, $\lambda = 220$ cm, $F_s = 2.4$ Hz.

Figure 1 shows the dependences (3) for that's frequencies of vibration in different depths of seawater. Depth $H = 30$ m (Fig. 1, *a*) corresponds to the planned experiment at the MHI RAS polygon. In this case, radar of the sound wave is possible only in X-band with $F_s = 28$ Hz. The diameter of the located membrane here is chosen $d = 20$ cm, the amplitude of its vibration is $b_m = 2$ cm. In the depths of $H = 150$ m (Fig. 1, *b*) are used vibration frequencies $F_s = 7.4$ Hz and 3.7 Hz (the possibility of radar in the L- and P-bands), are taken $d = 1$ m, $b_m = 10$ cm. Depth $H = 1000$ m (Fig. 1, *c*) corresponds to the known Japanese seismological experiment with

a real earthquake with a magnitude of 5.8 with a measurement of the sound pressure spectrum directly on the bottom [10]. Based on the need to capture at least part of the vibration spectrum $F_s = 2.4$ Hz and $F_s = 1$ Hz frequencies are used (corresponding to UHV and HV-bands), and as "membrane parameters" are taken $d = 100$ m and $b_m = 0.1$ m. For this case, on the figure 2 are built three-dimensional images of the pressure amplitude — in accordance with the two-dimensional graph on the Fig. 1, *c* with $F_s = 2.4$ Hz.

From Fig. 1 it is seen that the maximum amplitude of pressure in the "near" area (close $x = 0$) at the selected parameters of the membrane and the depth of the bottom strongly depends on the frequency of vibration. The first maximum formed in the waveguide at the lowest length of the sound wave $\Lambda_s \sim 4H$ (frequency $F_s = c/4H$) has an order of 0.15 from the main maximum, and decreases sharply with increasing frequency. Real earthquake is characterized by a wide spectrum of frequency: for example, at work [10] the measured spectrum of pressures is almost flat in the frequency range $Fs = (0.1 - 3)$ Hz, with a continuation of the measurements ~ 10 minutes. Important thing is: for radar observation earthquake focus at its depth $H = 1000$ m, for passing the sound on the waveguide "surface — bottom", it is necessary to register the frequency $F_s > c/4H \sim 0.4$ Hz — which includes all radar channels mentioned. However, in contrast to polygonal measurements, where the frequency of the simulation vibrator is determined by the wavelength of the radar — in the case of radar earthquake focuses follows, on the contrary, to select the wavelength

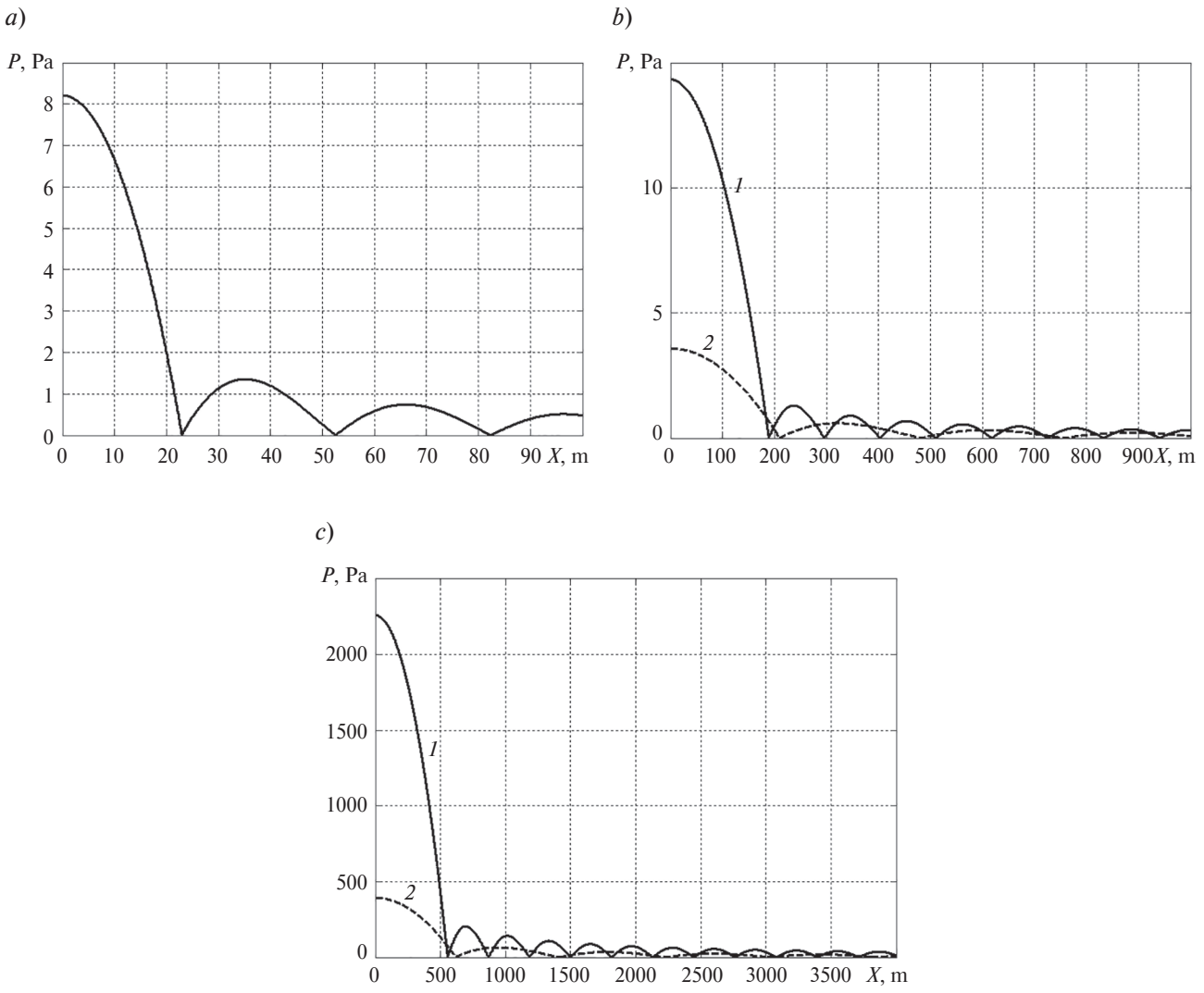


**Fig. 1**. Expected dependence of the pressure amplitude of the created low-frequency vibration wave in the conditions of the marine polygon with the use of a small-sized bottom vibrator (a vertical cut), $x$ — the distance from the point of surface above the vibrator. *a* — depth $H = 30$ m. Frequency of the vibrator $F_s = 28$ Hz. The sound with frequency $F_s = 7.4$ Hz does not pass through the waveguide; *b* — depth $H = 150$ m. *1* — frequency of the vibrator $F_s = 7.4$ Hz, *2* — frequency $F_s = 3.7$ Hz; *c* — Depth $H = 1000$ m. *1* — frequency of the vibrator $F_s = 2.4$ Hz; *2* — frequency $F_s = 1.0$ Hz

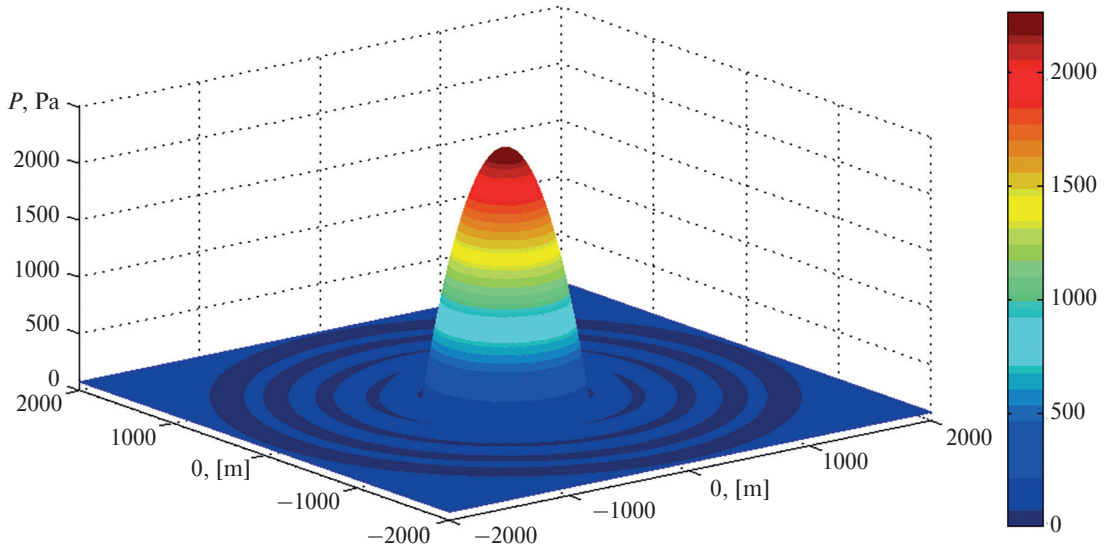


**Fig. 2**. Three-dimensional image of pressure amplitude around a small-scale earthquake focus at depth $H = 1000$ m, at a frequency $F_s = 2.4$ Hz (observing in UHV-range)

of the radar according to a specific area of pressure spectrum. In order to capture the right part of the spectrum in this case, it is necessary to use the UHV range in the "resonant" frequency $F_s = 2.4$ Hz. From Fig. 2 it is seen that in this case the expected quantity of the pressures from the observation of the focus of earthquakes (500–2000) Pa are two orders higher than those from the polygonal measurements at the selected vibrator parameters.

### 3. Amplitude of the surface vibration wave and comparison with the amplitude, sufficient for radar observation of the vibration wave on the background of wind waves

The calculations [1] allowed to connect the amplitude of the excitation wave (at the point above the vibrator) with the parameters of the bottom vibrator. It turns out that the excitation amplitude is

$$\xi_m = \frac{\pi F_s d}{H}\sqrt{\frac{b_m^3}{2\pi g}}, \tag{6}$$

and spatial dependencies for pressure (3), shown in Fig. 1 and Fig. 2, are equivalent to the relationship of the amplitude of the excitation wave to the horizontal distance (relative points over the vibrator), depth of water and vibration frequency $\xi_m(x, H, F_S)$, at the given diameter of the membrane ($d$) and the amplitude of its vibrations ($b_m$).

For expected polygonal measurements, for example $H = 30$ m, $d = 20$ cm, $b_m = 2$ cm. If the parametric "mechanism of amplification" of the surface vibration wave is not taken into account, then for the specified frequency of vibration $F_s = 28$ Hz from (6) at the point above the vibrator is obtained excitation amplitude $\xi_m \sim 0.02$ cm. By denoting the magnitude of the parametric amplification $Q$, it is obtained the amplitude $h_m = Q\,\xi_m$ perturbed on the surface of a vibration wave.

With radar of the sea surface, the level of the reflected signal is taken into account by the magnitude of the SESS (Specific Effective Surface Scattering), not depending on the equipment parameters and the distance. The wave number of the surface wave (basic diffract resonance) is $K_{res} = \dfrac{4\pi \sin\gamma}{\lambda}$, $\lambda$ — the length of radio wave, $\gamma$ — viewing angle of the surface. The spectral density of the surface vibration wave at its amplitude $h_m$ is $\Psi_h = \dfrac{h_m^2}{2K_{res}^2} = \dfrac{h_m^2}{8k_r^2 \sin^2\gamma}$, and its SESS: $\left(S^0\right)_{vibr} = \dfrac{\pi}{2} k_r^2 h_m^2 |q|^2 \cos^2\gamma \cdot \mathrm{ctg}^2\gamma$, $kr = 2\pi/\lambda$.

Spectral density is a small wind wave is $\left(S^0\right)_{wind} = \frac{\pi}{4} k_r^4 |q|^2 \operatorname{ctg}^4 \gamma \Psi_h\left(K_{res}\right)$, where $\Psi_h\left(K_{res}\right) \simeq \frac{a_0}{2\pi} K_{res}^{-4}$, $a_0 = 6.5 \times 10^{-3}$. In the gravity-capillary (GC) region the magnitude $a_0$ weakly depends on the speed of the wind, here this dependence is ignored (see selection of the similar works in [13]). Then $\left(S^0\right)_{wind} \simeq \frac{a_0 |q|^2}{64} \cos^4 \gamma$, and the relationship of SESS is as follows:

$$A = \frac{\left(S^0\right)_{vibr}}{\left(S^0\right)_{wind}} \simeq \frac{2 \cdot 10^4 \xi_m^2 Q^2}{\lambda^2 \cdot \sin^2 \gamma} \tag{7}$$

where $Q = h_m/\xi_m$ — the magnitude of the "parametric amplification" of the output vibration. Unfortunately, this value cannot be determined analytically, and measured (very rough) only in a laboratory experiment [1]. From (7) it turns out that three-fold exceedance of the SESS of the vibration wave over the SESS is ensured when $\xi_m \geq 2 \cdot 10^{-2} \frac{\lambda}{Q}$. That means, for points over the vibrator (Fig. 1, *a*) in the X-range ($\lambda = 3$ cm) necessary parametric amplification $Q > 10$, and for further ("waveguide") points necessary $Q > 10^2$ — if not to talk about the possibility of further amplifying the excitation wave by changing the vibration structure. The question of the influence of large waves is not considered here,— where the possibility of filtering regular (and, to a large extent, random) components of large waves using forward and inverse Fourier transforms from the obtained radar images with a known spatial spectrum of the useful signal is considered. In any case, if storm conditions are excluded, then in order to recognize the desired "portrait" of the underwater vibrator, apparently, there is a sufficient view of the excess of SESS vibrating overhead SESS of "resonant" wind wave.

### 4. The expected type of radar images from surface vibrating waves

On the aerospace side-looking radars, operating in the mode of selection of moving targets (interferometry with a longitudinal antenna base, see [7–9, 11, 12]), there is a possibility to isolate separately the amplitude of a signal (a module of complex magnitude) and the phase of a signal as an arctangent of the ratio of its quadrature components. In the "near" (hydrodynamic) area, as follows from the experiment [1], with a small amplitude $\xi_m$ (order of 0.1 cm) for produced a low-frequency vibration wave, over the source of vibration produces a narrow spotted standing waves, that's amplified by the parametric effect — "Faraday's ripple". Frequency of observed waves in 2 times lower frequencies $F_s$ of vibrator, and their length $\Lambda_v$, determined by the known of dispersion correspondence, on several orders of magnitude less than the length of the vibration wave: $\Lambda_v = \frac{2g}{\pi F_s^2}$ (here the surface tension is ignored). For example, at $F_s = 10$ Hz (which corresponds to the length of the sound wave $\Lambda_s = 150$ m) is $\Lambda_v = 6.2$ cm. Thus, in the bright channel of the ISAR (interference radar with synthesized aperture) directly above the vibrator is formed a bright spot, and around this spot is formed, according to the conducted experiment, short circle running waves. Their attenuation long the axis *x* cannot be ignored. Decrement of viscous attenuation is $\chi = 2\eta k_v^2$, where $\eta = 10^{-6} m^2/s$ — kinematic viscosity of water. In the gravitational interval of surface waves, $k_v^2 = \omega_v^4 / g^2$, and the decrement of attenuation for vibrating waves is $\chi = 32\pi^4 \cdot 10^{-6} \frac{F_v^4}{g^2} c^{-1}$. This means that the amplitude of the travelling wave decreases in *e* on the interval

$$\Delta l = \frac{2\pi F_v}{2\eta k_v^3} = \frac{g^3}{(2\pi)^5 \cdot 2\eta F_v^5} \ m \tag{8}$$

and in our case ($F_v = 10$ Hz), $\Delta l \approx 5$ m. Thus, in the ISAR high-speed channel, the vibration wave must be manifested as the current around the central spot with the speed, that's equal to its radial phase speed (the same as the central spot in the high-speed channel is not visible). This pattern is significantly different from the current on the wind waves, where the phases of the reflected signal in the formed areas of the small-structured sea surface (order 1 m) are random.

"Vibration spots", formed in polygon conditions ($H$ = 30 m, $F_s$ = 30 Hz, $F_v$ = 15 Hz, Fig. 1, *a*) in bright radar images and represented SESS of standing vibrating waves directly over the vibrator — should have a diameter of order 10m, and the surrounding halo of travelling waves is very narrow (order 1 m). If the energy of the radar allows, a bright standing waves rings should be observed at some distances (from points above the vibrator). From Fig. 1, *a* it is seen that the rings of nature "waveguide" should stand at points above the vibrator at distances $x$ = (40, 70, 100) m. In the conditions of deep water ($H$ = 1000 m) with using radar UHF-range, these distances are significantly increased — see Fig. 1, *c* and Fig. 2. However, drawing here in the polygonal conditions of the radar images of vibrating surface waves — for today it seems prematurely.

**5. Necessary parameters and features of SAR, performing monitoring of marine seismic situation**

The movement of the local reflector on the surface of the Earth is taken into account by introducing radial and tangential components of its speed in the functional, describing the behavior of the phase of the received signal at the same time while receiving and transmitting antenna are displacing. Detailed description of the method of signal processing on the ISAR with a longitudinal antenna base is available in [11]. Here it is necessary to repeat the basic positions, important for the case of monitoring of vibrating marine (underwater) sources.

The signal at the output of the antenna is:

$$\dot{U}(t) = U_0 \exp\left\{ j\left[ \varphi_n + \frac{4\pi}{\lambda} R_n - 2\pi t f_{dy} + \frac{2\pi}{\lambda R_n}\left(W_x - V_x\right)^2 t^2 \right]\right\},$$

where $f_{dy} = \dfrac{2V_y}{\lambda}\sin\gamma_n$ — doppler frequency shift from radially moving reflector; $W_x$ — tangential speed of antenna; $\varphi_n$ — phase of the reflector; $R_n$, $\gamma_n$ — inclined range and viewing angle of the reflector; $\lambda$ — signal wavelength, $t$ — time, calculated from the set position of the antenna phase center (PC). Ignoring the small tangential speed of the reflector by comparing the speed of the antenna and relating the phase shift $4\pi R_n/\lambda$ to the initial $\varphi_0$, for the sequence of $k$ pulses with the following period $Tr$, the signal is written as:

$$\dot{U}(k) = U_0 \exp j\left( \varphi_0 - 2\pi f_{dy} T_r k + \frac{2\pi W_x^2}{\lambda R_n} T_r^2 k^2 \right) = U_o \exp j\left[ \varphi_0 + ak\left( k - \frac{2t_V}{T_r} \right)\right], \quad (9)$$

where $a = \dfrac{2\pi W_x^2}{\lambda R_n} T_r^2$, $t_V = \dfrac{V_y R_n \sin\gamma_n}{W_x^2}$ — the axes shift of time because of reflector speed.

If four reflected impulses ($D_x = 4W_x T_r$) are accepted during the antenna passage time with its length $D_x$, then the offset of the antenna by half of its length takes place in two impulses, and the "doppler" increment of the signal phase during this time is $4\pi f_{dy} T_r$. The positions of the antenna PC are relative to the traverse when $k = \pm 1$. This means that the additional phase shift that arises from the antenna movement in both of its positions is relatively PC is the same and may be compensated. Indeed, from the expression (9) it follows that the difference of signals phase in this case is $\Delta\varphi = -4a\left( k - \dfrac{t_V}{T_r} \right)$, and at the point of the traverse ($k = 0$), $\Delta\varphi = 4a\dfrac{t_V}{T_r} = 4\pi f_{dy} T_r$. That means that the task is solved simply, using real aperture (RAR).

To obtain the required azimuthal resolution (especially from space) the synthesis of azimuthal directionality diagram is used — the algorithm for converting the received signal (9) with the support signal type: $\exp(-jan^2)$, the frequency of modulation of which changes linearly, relative to the points of the traverse $n = 0$, $\dfrac{\partial\psi}{\partial n} = -2an$:

$$\left\langle \dot{U}(k) \right\rangle = \int_{-N/2}^{N/2} \left[ \dot{U}\left(k - n\right) \exp\left( -jan^2 \right) \right] dn = U_0 \exp j\left[ \varphi_0 + ak\left( k - \frac{2t_V}{T_r} \right)\right] \int_{-N/2}^{N/2} \exp\left[ -2jan\left( k - \frac{t_V}{T_r} \right)\right] dn,$$

where $N = L_x/W_x T_r$ — the number of accumulated impulses, $L_x$ — the size of the synthesized aperture. The maximum number of accumulated impulses is determined by the real aperture, in this case $N_{\max} = 4\lambda R_n / D_x^2$.

Ignoring the change in the reflector range $R_n$, when moving the antenna to the element size $r_{x0} = \lambda R_n / D_x$, a synthesized azimuthal response of SAR is obtained:

$$\left\langle \dot{U}(k)\right\rangle = U_0 N \left|\frac{\sin\beta(k)}{\beta(k)}\right| \exp\left\{ j\left[ \varphi_0 + ak\left( k - \frac{2t_V}{T_r}\right)\right]\right\} \simeq U_0 N \exp\left[ -b\left( k - \frac{t_V}{T_r}\right)^2\right] \exp\left\{ j\left[ \varphi_0 + ak\left( k - \frac{2t_V}{T_r}\right)\right]\right\}, \quad (10)$$

where $\beta(k) = \frac{2\pi W_x T_r L_x}{\lambda R_n}\left( k - \frac{t_V}{T_r}\right)$, $b = \frac{2\pi W_x^2 T_r^2 L_x^2}{\lambda^2 R_n^2}$, and approximation $\left|\frac{\sin\beta}{\beta}\right| \to \exp\left( -\frac{\beta^2}{2\pi}\right)$ gives the opportunity to record the amplitude of the response in the form of a positive function without side petals.

Comparing expressions (9) and (10) can be seen that the phase multiplier is the same as without synthesis, but the point of maximum amplitude was shifted from the traverse ($k_0 = t_v/T_r$). The calculation shows that on the aircraft conditions the measurement of the interperiod difference around this point ($k_0 - 1$, $k_0 + 1$) gives $\Delta\varphi = 0$ already at radial speed of the reflector $V_y > 1$cm/s. Therefore, the presence of an azimuthal shift $x_v$ in this case excludes the possibility of measuring the speed $V_y$ on the response phase of the SAR in the center of the synthesized amplitude peak.

It is shown [11] that the task of measuring the radial speed of the reflector in the SAR is solved by antenna sectioning. That means to use of two distributed phase centers with a distance between them $l_x = D_x/2$ (Fig. 3).

For phase centers of the left and right sections, at the inputs of two synthesizers in the positions A and B antenna sections, the signals are formed:

$$\dot{U}_{1B}(k) = U(k)\exp j\left\{ \varphi_0 + a\left[ k^2 - \frac{2t_V}{T_r}(k-1)\right]\right\} \text{ and } \dot{U}_{2A}(k) = U(k)\exp j\left\{ \varphi_0 + a\left[ k^2 - \frac{2t_V}{T_r}(k+1)\right]\right\},$$

where $U(k)$ displays a real antenna diagram. At the exits of the synthesizers the responses are formed:

$$\left\langle \dot{U}_{1A}(k)\right\rangle = U(k) N_x \exp\left[ -b\left( k - \frac{t_V}{T_r}\right)^2\right] \exp\left\{ j\left[ \varphi_0 + a\left( k^2 - 2\frac{t_V}{T_r}(k-1)\right)\right]\right\} \quad (11)$$

$$\left\langle \dot{U}_{2A}(k)\right\rangle = U(k) N_x \exp\left[ -b\left( k - \frac{t_V}{T_r}\right)^2\right] \exp\left\{ j\left[ \varphi_0 + a\left( k^2 - 2\frac{t_V}{T_r}(k+1)\right)\right]\right\}.$$

In the case of a hybrid (sum-different) scheme of these responses (from the front antenna — with a delay of $2Tr$), at the exit of the hybrid scheme is obtained:

$$\dot{U}_{hyb} = \left\langle \dot{U}_{1B}(k)\right\rangle \pm \left\langle \dot{U}_{2A}(k)\right\rangle =$$

$$= U(k) N_x \exp\left[ -b\left( k - \frac{t_V}{T_r}\right)^2\right] \exp\left\{ j\left[ \varphi_0 + ak\left( k - 2\frac{t_V}{T_r}\right)\right]\right\} \times \left[ \exp\left( -2aj\frac{t_V}{T_r}\right) \pm \exp\left( 2aj\frac{t_V}{T_r}\right)\right], \quad (12)$$

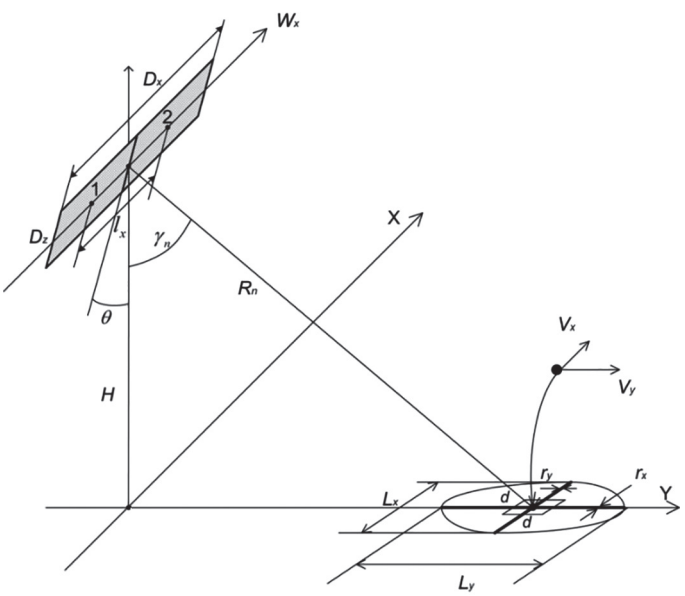


**Fig. 3**. Surface vision geometry in interference SAR. 1, 2 — sections of interferometer; $D_x$, $D_z$ — longitudinal and transverse dimensions of the antenna; $L_x$, $L_y$ — the sizes of the spotted real aperture; $r_x$ — azimuth resolution (longitudinal); $r_y$ — resolution of horizontal distance (transverse); $d$ — symmetrical averaging site; $V_x$, $V_y$ — the components of the site velocity

That means, the modules of summary and different responses (12) at the point of maximum amplitude are required quadrature components. Their sum $\left(U_{\cos}^2 + U_{\sin}^2\right)^{1/2}$ is used for the formation of amplitude radar images, and the magnitude $\Delta\varphi = \operatorname{arctg}\dfrac{U_{\sin}}{U_{\cos}} = 2a\dfrac{t_V}{T_r} = 2\pi f_{dy} T_r$ — for the formation of velocity radar images. In our case $f_{dy} = \dfrac{2V_y}{\lambda}\sin\gamma_n$, $V_y$ is the phase speed of the vibrating wave.

It should be noted that the information thus obtained on the value of azimuthal shift $t_V$ makes it possible to exclude it in both images (amplitude and velocity). In this way, unbiased radar images of vibration waves in the SAR, similar to the ones shown in Fig. 2, are formed. Functional scheme, explaining the sequence of operations, given in Fig. 4. It does not show the devices that ensure the synthesis (compression) of the signal at the range. Designed: 1, 2 — sections of SAR antenna; 3 — support signal generator; 4 — azimuthal synthesizers; 5 — delay for two periods of pulses; 6 — hybrid (sum-different) scheme; 7 — amplitude calculator; 8 — phase difference calculator; 9 — calculator-corrector of the parameters of the support signal (speed and height of the device, traverse coordinates); 10 — calculator-corrector of azimuthal coordinates of the moving object; 11 — formation of speed (different-phase) image; 12 — formation of bright (amplitude) images. The algorithm of the similar species is used on the German TerraSAR-X space radar, when forming images of land and sea moving objects [12].

Now let's consider the relations for the fluctuation sensitivity and the energy of the SAR in the formation of amplitude and velocity images of the sea surface. The background signal on the resolution element accumulates coherently, and the appratures noise is non-coherent, then for a brightness image, with a large number ($N > 20$) accumulated (on the resolution element) impulses, threshold ratio is as follows: $\dfrac{\Delta U_0^2}{\bar{U}_{\text{ш}}^2} = \dfrac{q_0}{\sqrt{N}}$, where $\overline{U}_{\text{ш}}$ — average-square deviation of the noise amplitude, $q_0$ — threshold coefficient. Enter the signal here $U_0^2$, relationship is received, where in the left part there is the working ratio of the signal/noise $q^2$, and in the denominator of the right part — the required threshold value of the signal intensity contrast $\Delta U_0^2 / U_0^2$: $q^2 = \dfrac{U_0^2}{\bar{U}_{\text{ш}}^2} = \dfrac{q_0}{\dfrac{\Delta U_0^2}{U_0^2}\sqrt{N}}$.

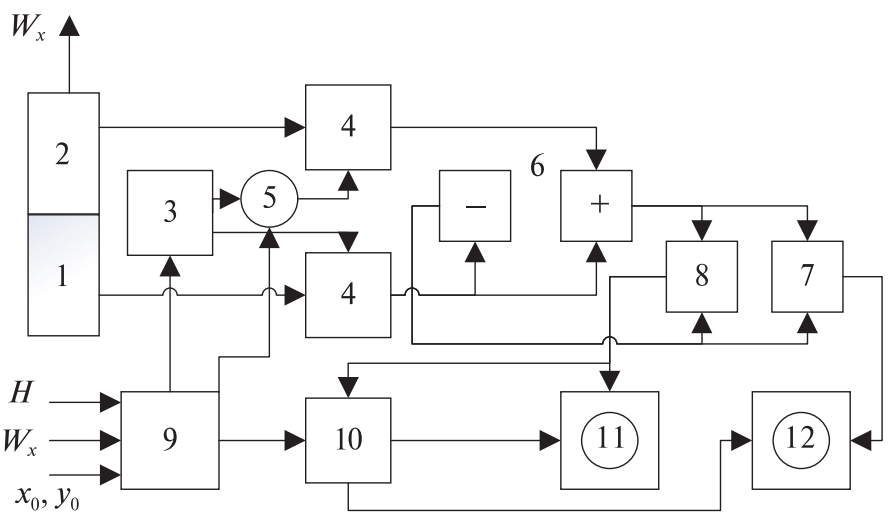


**Fig. 4**. Functional scheme that explains the method of generating amplitude and velocity images in the ISAR with compensation (exclusion) of the azimuthal shift of a moving object

Usually: $10\lg(1 + K_{\text{пор}}) = 1$ dB, $K_{\text{пор}} = \Delta U_0^2 / U_0^2 = 0.26$. The number of accumulated realizations of noise is determined by the relationship between the synthesized and real dimensions of the antenna: $N \approx \frac{L_x}{D_x}$, $L_x >> D_x$. Therefore, at the set threshold $q_0 = 3$ and $K_{\text{пор}} = 1$ dB, in the SAR is received $q^2 \approx 10\sqrt{\frac{D_x}{L_x}}$. Thus, thanks to the coherent accumulation of impulses on a small area, it is possible to form a brightness image of a weak-reflecting surface with a good resolution. It turns out that under the conditions of airborne SAR, at $D_x = 1$ m, $L_x = 100$ m — on the background can work in full focus mode with a working ratio background/noise order of units.

The fluctuation error in measuring the different-phase increment depends on the steepness phase-velocity characteristics $\partial\psi_n/\partial V_y$, the number of $N$ incoherent accumulated noise counts, and also from the module $|\rho_n|$ correlation coefficient of the accumulated signal in relation to noise:

$$\sigma_V = \sqrt{\frac{1}{|\rho_n|^2} - 1} \Big/ \frac{\partial\psi_n}{\partial V_y}\sqrt{N}. \tag{13}$$

In case of signal / noise $q >> 1$ (background is ignored) can be counted $|\rho_n| = \frac{q^2}{1+q^2}$, $\frac{\partial\psi_n}{\partial V_y} = \frac{8\pi T_r \sin\gamma_n}{\lambda}$, then from the relation (10) there is a fluctuating-speed sensitivity, which responds to the resolution of the "point" reflector:

$$\sigma_{V0} = \frac{\lambda}{2\pi T_r q\sqrt{2N_0}\sin\gamma_n}. \tag{14}$$

In airborn SAR ($\lambda = 3$ см, $T_r = 10^{-3}$ $c$, $\gamma = 60^\circ$, $N \sim 10^2$) with $q = 10$, we would have received such a high sensitivity $\sigma_{v0} \sim 2$ cm/s, with a resolution of ~ 1 m on both axes.

In the case of the background reflector (sea currents), the situation changes significantly. The number of independent background reports on a symmetric area of size $d >> r_x, r_y$, $N = \frac{2d^2}{D_x r_y}$, and the coefficient $q$ represents the ratio of the background / own noise, then

$$\sigma_V = \frac{\lambda\sqrt{D_x r_y}}{8\pi T_r d\sin\gamma_n}. \tag{15}$$

This means that in the specified parameters of the aviation SAR, speed sensitivity $\sigma_V \sim 2$cm/s can be obtained only at a high ratio of background / noise ($q = 10$) and on the sites of size not less than $d \sim 10$ m on the both axis.

SAR energy is calculated as a standard method, based on a well-known relationship $P_2 = P_1\frac{G_{a1}G_{a2}\lambda^2 S_t}{(4\pi)^3 R_n^4} \geq q^2 k T_{\text{ш}}\Delta f$, where $P_1$, $P_2$ — power of the emitted and received short pulses (without taking into account the coefficient of compression at a distance), $S_t$ — is ESS of "point" reflector, $\Delta f$ — spectrum width of the signal, $G_{a1} = \frac{4\pi D_x D_z}{\lambda^2}$ — amplification of antenna on the transmission, $G_{a2} = \frac{4\pi L_x D_z}{\lambda^2}$ — amplification of the synthesized antenna on the receiver, $D_z$ — vertical size of the antenna, $T_n$ — equivalent noise temperature of the receiver, $k = 1.37 \cdot 10^{-23}$ $W/K \cdot$ Hz — Boltzmann constant. The width of the zone $L_y$ corresponds to the angular width of the antenna diagrams (determined by the size $D_z$), the azimuthal width $L_x$ is determined by the size of $D_x$, and the angle of inclination of the antenna plane $\theta$ is consistent with the average angle of vision $\gamma_n = (\pi/2 - \theta)$ — see Fig. 3.

In this case, the impulse power $P_1 \geq \frac{4\pi q^2 k T_{ø} R_n^4 \lambda^2 \Delta f}{D_z^2 D_x L_x S_t}$. Average power is inversely proportional to the compression coefficient $B = \Delta f \tau_p$ and relative pulse duration $Q = \frac{T_r}{\tau_p}$, and the maximum pulse period $T_r$ is determined by the necessity of maintaining the coherence of the background. That means the receiving two impulses during the flight of the antenna size $D_x$: $T_r \leq \frac{D_x}{2W_x}$, $W_x$ — antenna speed. The result is average power $\bar{P}_1 = \frac{P_1}{BQ} \geq \frac{8\pi q^2 k T_{ш} R_n^4 \lambda^2 W_x}{D_z^2 D_x^2 L_x S_t}$. The point reflector and a background reflector will be replaced, then we will take into account the resolution of the area with full focusing $S_t = S^0 r_x r_y = S^0 \frac{c\lambda R_n}{2\Delta f L_x \sin\gamma_n}$, where $S^0$ — SESS of surfaces. Than

$$\bar{P}_1 \geq \frac{16\pi q^2 k T_{ш} \Delta f H^3 \lambda W_x \sin\gamma_n}{D_z^2 D_x^2 S^0 c \cos^3\gamma_n}. \quad (16)$$

For the formation of radar images of the sea surface with the plane using $q = 10$, $\Delta f = 3 \times 10^8$ Hz, $\gamma_n > 60°$, then at $kT_{ш}\Delta f = 10^{-20}$ *W* and wavelength $\lambda = 3 \times 10^{-2}$ m, as well as vertically polarization of antenna (on the transmitter and receiver), should take the magnitude of SESS $S^0 = 10^{-3}$. At $H = 10^4$ m, $W_x = 10^2$ m/s, $D_x = 2$ m, $D_z = 0.2$ m, average power $\bar{P}_1 \geq 6$ W, and relative pulse duration $M \sim 10^2$, the required impulse power is $P_p \sim 600$ W.

Thus, the basic parameters of the aircraft SAR were revealed: resolution of both axes of order 1 m with contrast-bright fluctuation sensitivity of the radar images better than 1 dB, speed fluctuation sensitivity $\sigma_V \sim$ 2cm/s on a square size $d \sim 10$ m and impulse power of order 1 kW. Width zone review composes $L_y \sim 3H$ (not less than 30 km). It should be noted that the resulting value $\sigma_V \sim 2$ cm/*s* for velocity fluctuation sensitivity means that the threshold phase speed of the vibrating waves is not less than ~ 6 cm/s. In a in-situ experiment with the frequency of the vibrator $F_s \sim 30$ Hz and the vibration wave $F_v \sim 15$ Hz — its phase speed is ~ 25 cm/s. That means that at velocity radar image, as and at amplitude image, vibrational wave must be well visible against the background of wind waves.

### 6. Short conclusions

1. Adopted admissions about the parameters of the flat bottom, about the small size of the bottom vibrator to compare with the longitudinal of emitted sound wave and about the depth of the water, comparable to the long sound wave, lead to a certain pattern for parametrically excited surface vibration waves of small length. In the near area (close to the points above the vibrator) the amplitude of the vibration wave is maximum, in the far area the amplitude can be significant at certain distances (waveguid distribution of sound).

2. At a small depth of water (20–40 m) is a complete simulated in-situ experiment with the participation of a bottom vibrator and aircraft radar, using an interferometer with a longitudinal antenna base with the necessary binding of the radar wavelength (X-band) to the vibration frequency (30Hz).

3. Vibration spectrum of the real epicenter of earthquakes, measured at a depth of 1000 m, had a flat shape at the limits (0.1–3 Hz). Radar of a similar epicenter is possible when the wavelength of the radar is more than 1 m (UHV and HV ranges).

4. Radar images of vibrating waves, formed in the bright and speed channels of modern SAR, must have a different shapes and, according to the calculations, the vibrating wave must be well separated from the wind waves.

### 7. Acknowledgements

The authors are deeply grateful to the reviewers, whose comments allowed not only to improve the text of the article (in particular — drawings), but also to eliminate the fundamental error in the original text.

## 8. Funding

This research was performed in the Shirshov Institute of Oceanology of RAS within the framework of the State Task (Theme No. 0128–2021–0003).

## References

1. *Pereslegin S.V.*, *Levchenko D.G.*, *Karpov I.O.* The vibration wave on the water surface: parametric excitation and radar observation. *Fundamental and Applied Hydrophysics*. 2021, 14, 2, 39–53 (in Russian). doi: 10.7868/S2073667321020040
2. *Rabinovich M.I.*, *Trubetskov D.I.* Introduction to the theory of vibrations and waves. *Moscow*, *Nauka*, 1984, 560 p. (in Russian).
3. *Levin B.V.*, *Nosov M.A.* Physics of tsunamis and related phenomena in the ocean. *Moscow*, *Yanus-K*, 2005, 360 p. (in Russian).
4. *Shenderov E.L. Sound emission and scattering. Leningrad. Sudostroyeniye*. 1989, 301 p. (in Russian).
5. *Razin A.V.*, *Sobisevich A.L.* Geoacoustics of layered medium. *Moscow*, *IFZ by O. Yu. Shmidt RAS*. 2012, 210 p. (in Russian).
6. *Isakovich M.A.* General acoustics. *Moscow*, *Nauka*, 1973, 436 p. (in Russian).
7. *Toporkov J.V.*, *Perkovic D.*, *Farquhanson G.*, *Sletten M.A.*, *Frasier S.J.* Sea surface velocity vector retrieval using dual-beam interferometry: first demonstration. *IEEE Transactions on Geoscience Remote Sensing*. 2005, 43, 11, 2494–2502. doi: 10.1109/TGRS.2005.848603
8. *Romeiser R.* The future of SAR-based oceanography: High-resolution current measurements by along-track interferometry. *Oceanography*. 2013, 26, 2, 92–99. doi: 10.5670/oceanog.2013.37
9. *Verba V.S.*, *Pluschev V.A.*, *Manakov V. Yu.* The use of an aviation SAR system operating at low frequencies for excitation and subsurface sounding. *Proceedings of NTO RES n.a. A.S. Popov* "*Ultrawideband signals and ultrashort pulses in radar, communications and acoustics*". *Suzdal — Moscow*, 2005. P. 89–94 (in Russian).
10. *Hiuoyuki Matsumoto*, *Toshinory Kimura*, *Shuhei Nishida*, *Yuya Machida*. Experimental evidence characterizing pressure fluctuations on the sea floor-water interfaced induced by an earthquake. *Scientific Reports*. 2018, 8, 10. doi: 10.1038/s41598-018-34578-2
11. *Pereslegin S.V.*, *Khalikov Z.A.* Signal processing in synthestic-aperture radars during the formation of the Earth-surface velocity fields. *Radiophysics and Quantum Electronics*. 2015, 57, 700–710. doi: 10.1007/s11141-015-9556-7
12. *Cassola M.R.*, *Iraola P.P.*, *De Zan F.*, *Scheiber R.*, *Reigber A.*, *Geudtner D.*, *Alberto Moreira*. Doppler-related distortions in TOPS SAR images. *IEEE Transactions on Geoscience and Remote Sensing*. 2015, 53, 1. doi: 10.1109/TGRS.2014.2313068
13. *Pereslegin S.V.*, *Karpov I.O.*, *Khalikov Z.A.* Two-position quasi-mirror radar of the sea surface: Principles of microwave scattering and possibilities of solving Oceanology problems from space. *Oceanology*. 2017, 57, 639–647. doi: 10.1134/S0001437017050149
14. *Pereslegin S.V.*, *Khalikov Z.A.*, *Karpov I.O.* Model of formation of fields of wind and internal waves in IRSA with a longitudinal antenna base. *Proceedings of XXIX All-Russian Symposium* "*Radiolokatsionnoye issledovaniye prirodnykh sred*". *St. Petersburg*, *A.F. Mozhaysky VKA*, 2019.

## Литература

1. *Переслегин С.В.*, *Левченко Д.Г.*, *Карпов И.О.* Вибрационная волна на поверхности воды: параметрическое возбуждение и радиолокационное наблюдение // Фундаментальная и прикладная гидрофизика. 2021. Т. 14, № 2. С. 39–53. doi: 10.7868/S2073667321020040
2. *Рабинович М.И.*, *Трубецков Д.И.* Введение в теорию колебаний и волн. М.: Наука, 1984. 560 с.
3. *Левин Б.В.*, *Носов М.А.* Физика цунами и родственных явлений в океане. М.: Янус-К, 2005. 360 с.
4. *Шендеров Е.Л.* Излучение и рассеяние звука. Л.: Судостроение, 1989. 301 с.
5. *Разин А.В.*, *Собисевич А.Л.* Геоакустика слоистых сред. М.: ИФЗ им. О.Ю. Шмидта РАН, 2012. 210 с.
6. *Исакович М.А.* Общая акустика. М.: Наука, 1973. 436 с.
7. *Toporkov J.V.*, *Perkovic D.*, *Farquhanson G.*, *Sletten M.A.*, *Frasier S.J.* Sea surface velocity vector retrieval using dual-beam interferometry: first demonstration // IEEE Transactions on Geoscience Remote Sensing, Nov. 2005. Vol. 43, No 11. P. 2494–2502. doi: 10.1109/TGRS.2005.848603

8. *Romeiser R.* The future of SAR-based oceanography: High-resolution current measurements by along-track interferometry // Oceanography. 2013. Vol. 26, No 2. P. 92–99. doi: 10.5670/oceanog.2013.37
9. *Верба В.С.*, *Плющев В.А.*, *Манаков В.Ю.* Применение авиационного РСА комплекса, работающего в широком диапазоне частот, для поверхностного и подповерхностного зондирования // Труды НТО РЭС им. А.С. Попова «Сверхширокополосные сигналы и сверхкороткие импульсы в радиолокации, связи и акустике». Суздаль — Москва, 2005. С. 89–94.
10. *Hiuoyuki Matsumoto*, *Toshinory Kimura*, *Shuhei Nishida*, *Yuya Machida*. Experimental evidence characterizing pressure fluctuations on the sea floor-water interfaced induced by an earthquake // Scientific Reports. 2018. Vol. 8, No 10. doi: 10.1038/s41598-018-34578-2
11. *Переслегин С.В.*, *Халиков З.А.* Обработка сигналов в радиолокаторах с синтезированной апертурой при формировании скоростных полей поверхности Земли // Известия ВУЗов. Радиофизика. 2014. Т. LVII, № 10, С. 784–796.
12. *Cassola M.R.*, *Iraola P.P.*, *De Zan F.*, *Scheiber R.*, *Reigber A.*, *Geudtner D.*, *Alberto Moreira*. Doppler-related distortions in TOPS SAR images // IEEE Transactions on Geoscience and Remote Sensing. 2015. Vol. 53, No 1. doi: 10.1109/TGRS.2014.2313068
13. *Переслегин С.В.*, *Карпов И.О.*, *Халиков З.А.* Двухпозиционная квазизеркальная радиолокация морской поверхности: механизмы СВЧ-рассеяния и возможности решения океанологических задач из космоса // Океанология. 2017. Т. 57, № 5. С. 710–719. doi: 10.7868/S0030157417050057
14. *Переслегин С.В.*, *Халиков З.А.*, *Карпов И.О.* Модель формирования полей ветровых и внутренних волн в ИРСА с продольной антенной базой // Труды XXIX Всероссийского симпозиума «Радиолокационное исследование природных сред». СПб.: ВКА им. А.Ф. Можайского, 2019.